DNA molecules on periodically microstructured lipid membranes: Localization and coil stretching

Marion B. Hochrein,[1] Judith A. Leierseder,[1] Leonardo Golubović,[2] and Joachim O. Rädler[1]
[1]*Department für Physik, Ludwig-Maximilians-Universität, Geschwister-Scholl-Platz 1, D-80539 München, Germany*
[2]*Physics Department, West Virginia University, Morgantown, West Virginia 26506-6315, USA*
(Received 8 October 2006; published 1 February 2007)

We explore large scale conformations of DNA molecules adsorbed on curved surfaces. For that purpose, we investigate the behavior of DNA adsorbed on periodically shaped cationic lipid membranes. These unique membrane morphologies are supported on grooved, one-dimensionally periodic microstructured surfaces. Strikingly, we find that these periodically structured membranes are capable to stretch DNA coils. We elucidate this phenomenon in terms of surface curvature dependent potential energy attained by the adsorbed DNA molecules. Due to it, DNA molecules undergo a localization transition causing them to stretch by binding to highly curved sections (edges) of the supported membranes. This effect provides a new venue for controlling conformations of semiflexible polymers such as DNA by employing their interactions with specially designed biocompatible surfaces. We report the first experimental observation of semiflexible polymers unbinding transition in which DNA molecules unbind from one-dimensional manifolds (edges) while remaining bound to two-dimensional manifolds (cationic membranes).

DOI: 10.1103/PhysRevE.75.021901 PACS number(s): 87.14.Gg, 87.15.He, 82.37.Rs, 82.35.Gh

I. INTRODUCTION

There has been a lot of recent experimental and theoretical interest in the properties of the DNA-cationic lipid complexes used for DNA transfection in gene therapies of cancer [1]. These prominent biomaterials were recently shown to form interesting condensed structures and exemplify unique and unusual liquid crystalline states of matter [2–7]. A special role in this area is played by the cationic-lipid membranes supported on solid surfaces [8–10], due to the fact that naturally anionic DNA adsorbed on such membranes is laterally mobile [9,10]. In a recent paper [11] and here in more detail, we explore the behavior of DNA molecules adsorbed on cationic-lipid membranes prepared on grooved, periodically structured substrates. We demonstrate a striking ability of these periodically microstructured membranes to stretch DNA coils. Underlying this phenomenon is an interesting DNA localization transition promising to play an important role in future biophysical and biotechnological studies.

In this paper, we address a basic polymer physics question: What is the character of the large-scale conformations of semiflexible polymers, such as DNA, that are adsorbed on *curved* surfaces, such as the periodically structured surfaces studied here? Previous experiments have been focused on the DNA behavior on planar surfaces [9,10]. These studies have exemplified some of the fundamental statistical physics laws, such as the statistics of two-dimensional (2D) self-avoiding random walks that applies to DNA molecules confined to a plane [9,10]. However, prior to our recent paper [11] (describing briefly findings of this study), no much was known (both experimentally and theoretically) on how semiflexible polyelectrolytes such as DNA behave on curved surfaces under realistic situations involving common binding forces, e.g., the screened electrostatic forces. To address these statistical and polymer physics questions, here we explore the conformations and dynamics of DNA molecules adsorbed on cationic lipid membranes supported on periodically structured surfaces made of the cyclic olefin copolymer.

We experimentally reveal that the semiflexible polymers adsorbed on periodic membranes are involved in conceptually and practically interesting phenomena of polymer localization and coil stretching. Our study highlights a previously not anticipated significant role of surface curvature potentials in governing conformations of biomacromolecules. On the practical side, as a contribution to an ongoing quest to unfold the coiled and therefore inaccessible state of DNA in its natural three-dimensional (3D) environment [12], our study initiates a new venue for controlling conformations of semiflexible biopolymers by employing their interactions with specially structured biocompatible surfaces. To study interactions of DNA with other biomolecules it is frequently necessary to unfold and stretch the coiled and therefore inaccessible state of DNA in its 3D environment. Within our approach, DNA can be easily brought in large amounts onto our periodic membranes and the stretched DNA molecules are freely exposed to a large surrounding water medium and all the molecules dissolved in it. Our discovery may thus facilitate more direct, high throughput protocols, and studies of fundamental biological processes involving DNA and other biomolecules.

The layout of this paper is as follows: In Sec. II, we describe materials and methodology used as well as our experimental strategies employed in exploring DNA conformations on curved surfaces. In Sec. III, we describe the geometry of our grooved periodic surfaces, and investigate the dynamics and conformations of DNA molecules on periodic membranes. The physical origin of the observed stretching of DNA coils is addressed in Sec. IV. We summarize and further discuss our findings in Sec. V.

II. MATERIALS AND METHODS

To explore the behavior of DNA adsorbed on curved surfaces we employ cationic lipid membranes supported on

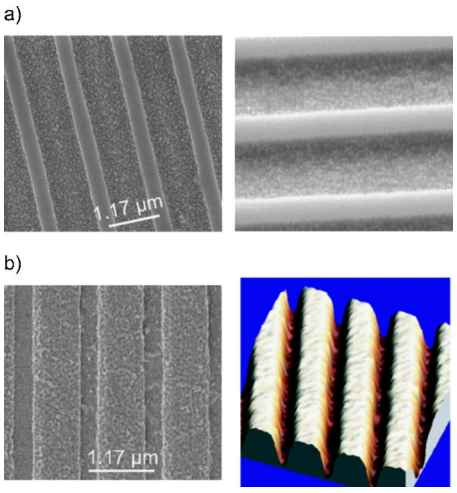

FIG. 1. (Color online) (a) SEM images of a section of the silicon master used for imprinting. (b) Left panel, SEM image, and AFM perspective image (right panel, color online) of a small section of the imprinted grooved surface of COC. Both the master and the surface are nearly one-dimensionally periodic, with the average period $L=1.17$ μm.

periodically structured surfaces of the cyclic olefin copolymer (COC). One-dimensional (1D) periodic arrangements of long grooves (grids) with the average period $L=1.17$ μm [Fig. 1(b)], were imprinted into COC foils [13]. The imprinting was done by using a silicon master [Fig. 1(a)] produced by holographic methods and subsequent reactive ion etching of (100) silicon wafers [14]. To imprint the grooves, the master was pressed into COC foil (with a 80 g weight) for 10 h under 150 °C (above the COC glass transition temperature of 135 °C). The master was removed after cooling the surface to 70 °C. The COC surfaces prepared by this approach are nearly periodic, as detailed in Sec. III. We covered the grooved COC surfaces by fluid membranes prepared from mixtures of neutral lipid 1,2Dioleoyl-sn-Glycero-3-Phosphocholine (DOPC) and cationic lipid 1,2Dioleoyl-3-Trimethylammonium-Propane (DOTAP), Avanti Polar Lipids (Alabaster, AL, USA), by the solvent exchange method [15]. For this purpose, we glued the structured COC foil (180 μm thickness) to the microfluidic chamber sold by ibidi Gmbh (Munich, Germany). As detailed in [16], the membranes used here form a lipid bilayer supported on COC, with a lipid diffusion constant $=0.8\pm0.1$ $\mu m^2/sec$.

The use of the lipid mixture allows us to vary the strength of DNA-membrane electrostatic interactions by using membranes with different relative fractions of DOTAP. In our study, we used λ-phage DNA bought from Roche (Mannheim, Germany) and diluted to a concentration of 0.1 μg/ml. 127 μl of a 0.5 μM Toto-1 fluorescent dye solution was added to 200 μl of DNA and 1 ml of 10 mM Hepes pH 7.0 was also added. The solution was heated to 50 °C for 20 min. This results in a labeling ratio of 1:5, and a DNA contour length of 21 μm, [17].

Our experimental strategy was the following: The anionic DNA molecules were deposited on the supported cationic membranes from a salt-free buffer solution (10 mM Hepes, pH 7.0). The absence of salt provides a rapid deposition of the DNAs, yet it makes them practically immobile after they deposit. To activate DNA dynamics, the electrostatic interactions are weakened (screened) by exchanging the solvent with a NaCl water solution (10 mM Hepes, 30 mM NaCl, 5 mM Vit C, pH 7.0). The post-deposition dynamics and conformations of the DNA molecules adsorbed onto the membranes supported on the grooved 1D periodic solid surfaces, were visualized by an inverted fluorescence microscope (FM), Axiovert 100 M (Carl Zeiss, Oberkochen, Germany), resolution 0.4 μm, equipped with a 100× oil immersion objective (100 Plan Neofluar, N.A. 1.3, Carl Zeiss, Oberkochen, Germany). The same optical system was used to check the quality of the lipid layer on the COC foil. Images were taken with a CCD camera (Coolsnap HQ, Photometrics, Roper Scientific Inc., Tucson, USA). Image analysis was done with Igor Pro 4.0 (Wavematrics, Portland, USA).

III. SURFACE GEOMETRY AND CONFORMATIONS OF DNA ON PERIODIC MEMBRANES

Geometrical properties, such as the curvature of the grooved periodic surfaces we employed to support fluid membranes, will be shown here to play an essential role in governing DNA conformations. Of special interest are highly curved surface sections, the inward curved edges seen in Fig. 2. Their possible role has been highlighted in our recent paper [11]. The COC surface morphology is explored here by scanning electron microscopy (SEM) and atomic force microscopy (AFM) techniques, see Figs. 1 and 2. The COC surface is shaped to form a nearly periodic rid of grooves, with the average period $L=1.17$ μm. The AFM image of a small subsection of the periodic COC surface seen in Fig. 2(a) depicts a to-scale cross-sectional profile $h(x)$ of two consecutive grooves along the direction perpendicular to the grooves. [Here, we tacitly ignore a substantially weaker y dependence of the surface profile. See, however, Sec. IV end.]. For the following discussions, it will be significant to express the surface period as $L=L_{short}+L_{long}$. Here, $L_{long}\approx 950-1000$ nm is the distance between neighboring *inward* curved edges that are in adjacent grooves, whereas $L_{short}\approx 200$ nm is the distance between the two inward curved edges that are in the same groove, see Fig. 2(a).

In Fig. 2(b), we give a close view on the surface behavior in the vicinity of an inward curved surface edge, in terms of the surface profile $h(x)$, local surface slope angle $\Theta(x)=\tan^{-1}(dh/dx)$, and

$$C=\frac{d\Theta}{ds}=\frac{\frac{d^2h}{dx^2}}{\left[1+\left(\frac{dh}{dx}\right)^2\right]^{3/2}},$$

the local surface curvature C along x direction. Across the inward curved edge, $\Theta(x)$ increases rapidly by $\Delta\Theta\approx 1$ rad, yielding a very strong peak (with $C>0$) in the C *vs* x plot, corresponding to $1/C=R=20-30$ nm, or even smaller, as this size ≈AFM tip radius. By $1/C=R=w/\Delta\Theta$, the corresponding width of the inward edge is small;

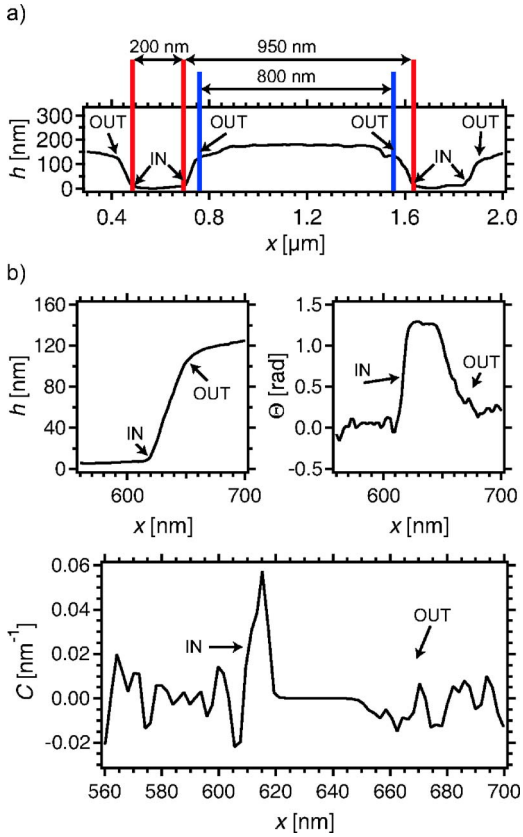

FIG. 2. (Color online) (a) Cross sectional AFM image giving surface profile $h(x)$ of two grooves of the imprinted COC surface, with inward (IN) and outward (OUT) curved sections (edges). We label here the physically significant length scales: $L_{long} \approx 950 - 1000$ nm, the distance between neighboring *inward* curved edges that are in adjacent grooves, and $L_{short} \approx 200$ nm, the distance between the two inward curved edges that are in the same groove. (b) Close-up views on the surface behavior in the vicinity of one of the surface inward edges [for x around 600 nm in (a)], in terms of the surface profile $h(x)$, local surface slope angle $\Theta(x)$, and $C(x)$, the local surface curvature (along x direction), see the text.

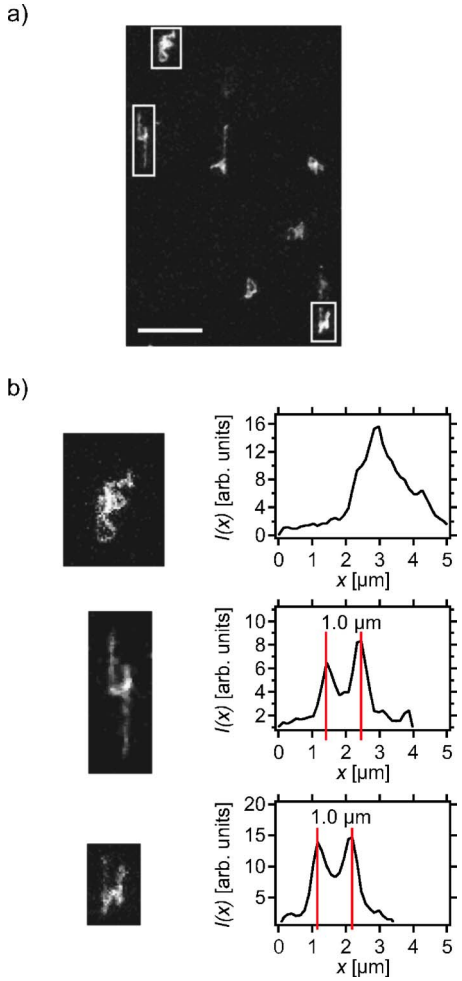

FIG. 3. (Color online) (a) FM images of DNA molecules on periodically structured membrane with 5% of DOTAP, illustrating the Stage 1 of the DNA dynamics (here, at $t=48$ min after exchanging the solvent with the salt solution, see the text); scale bar $=10$ μm. (b) For a few selected molecules, we give the projected intensity profiles versus x, obtained by summing local image intensity $I(x,y)$ over y (within a domain containing only the selected single molecules).

$w = R\Delta\Theta = 20-30$ nm. In contrast to this, the outward curved edge in Fig. 2(b) has a much bigger width, i.e., smaller curvature, and its would-be peak in the C *vs* x plot (with $C<0$) is depressed by a background of curvature variations (of *both* signs) due to local surface roughness.

We now proceed to describe the post-deposition dynamics and conformations of the DNA molecules adsorbed onto fluid membranes supported on the grooved 1D periodic solid surfaces. Initially, just after the deposition, the adsorbed DNA molecules form 2D globules sitting on the membranes. From our experiments, we find a strong dependence of the subsequent DNA dynamics and shapes on the amount of the charged lipid DOTAP. This is documented in Figs. 3, 4, 6, and 7 here. We reveal a striking conformational behavior, the DNA coil stretching phenomenon, best seen on membranes with 5% of DOTAP at 30 °C [see Figs. 3 and 4]. The observed DNA stretching process proceeds as a sequence of two experimentally discernable stages of single molecule dynamics: First, the DNA molecules from the initial globules get efficiently sucked into nearby grooves, on a 25–50 min time scale (*Stage 1*, see Fig. 3). During the Stage 1, DNA globules evolve into a configuration typically including two long DNA sections (arms) sucked into the surface grooves, which are connected by about 1 μm long DNA *crossing* from one to another groove. See Fig. 3(a), in which some DNAs are still globular whereas other have already assumed the arms-and-crossing configuration [in Figs. 3 and 4, the grooves (invisible) run vertically, and the DNA crossings are horizontal]. After Stage 1, the DNA dynamics slows down. It assumes the character of the one-dimensional reptationlike motion of the DNA molecule, which moves along its contour directed by the grooves (*Stage 2*, seen in Fig. 4). As seen from the sequence of snap shots of the DNA molecule in Fig. 4(b), this motion eventually leads to a pullout of one of the two DNA arms in the grooves, so the entire DNA molecule eventually slips into a single groove. After this apparently irreversible extinction of the DNA crossing between the grooves, which typically occurs on the time scale of several

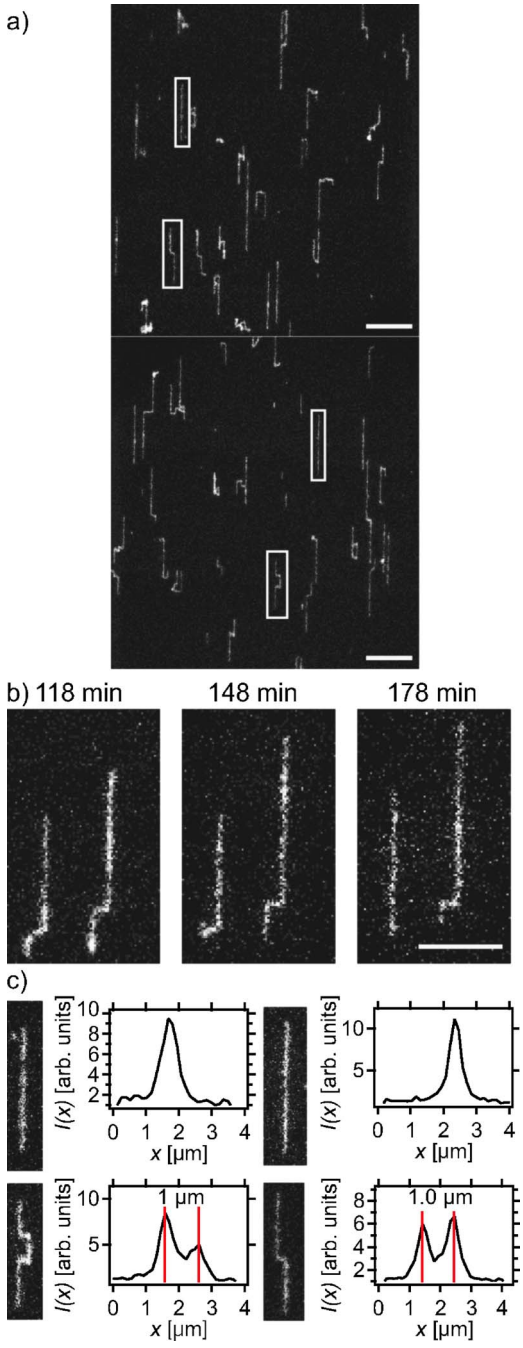

FIG. 4. (Color online) (a) FM images of DNA molecules on periodically structured membrane with 5% of DOTAP illustrating the Stage 2 of the DNA dynamics on two different surface sections, upper panel at $t=264$ min, lower panel at $t=369$ min; scale bar $=10$ μm. The surface grooves (invisible) here would appear as vertical grid with 1.17 μm period. At $t\approx 5$ h, the average DNA projected length along the grooves $L_y \approx 10.5$ μm (by including all molecules, some of them having U-turns and crossings reducing the L_y). The DNA molecules adsorbed into single grooves (and thus having no crossings) have projected lengths $\approx 13-14$ μm. (b) A sequence of snap-shots with a DNA molecule that initially has two arms in two grooves, and then it slips into a single groove, via a reptationlike motion [here, scale bar=5 μm]. (c) For a few selected molecules, we give the projected intensity profiles versus x [see Fig. 3(b) caption].

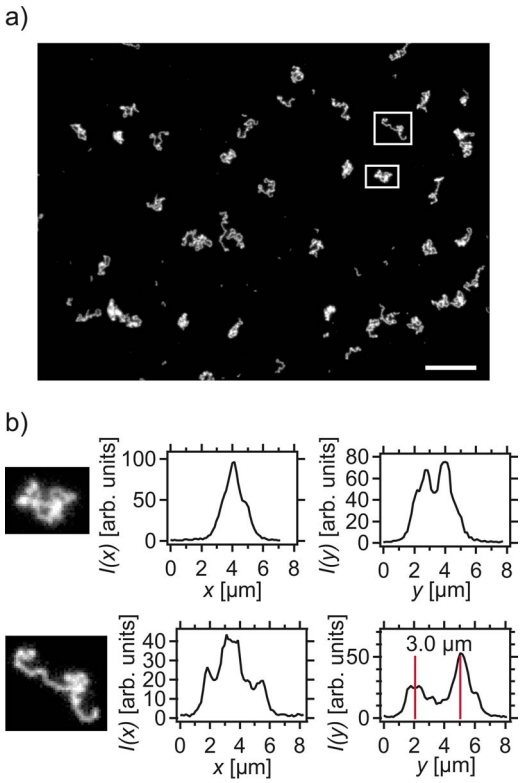

FIG. 5. (Color online) (a) FM images of DNA molecules on planar membrane with 5% of DOTAP, (here at $t=140$ min; qualitatively the same images are obtained at *any* $t>25$ min); scale bar $=10$ μm. (b) For a few selected molecules, we give the projected intensity profiles $I(x)$ [intensity projected along y-direction] and $I(y)$ [intensity projected along x-direction].

hours, the entire DNA molecule gets completely adsorbed into a single long groove. A global view on the Stage 2 of the DNA dynamics is captured in Fig. 4(a), in which some DNA molecules still exhibit the two arms connected by crossings between grooves, whereas other DNA molecules have already slipped into single grooves and thus stretched.

The curved periodically structured membranes are thus capable to orient and stretch long DNA molecules. This is in striking contrast to the conformational behavior of DNA molecules on planar membranes which maintain coiled random walk like shape at long times, as illustrated by our images in Fig. 5 on planar membranes with 5% of DOTAP. What is the physical mechanism underlying this DNA stretching that we revealed on curved periodic membranes with 5% of the charged lipid? In the present system, it would be natural to correlate this phenomenon to the electrostatic binding of the DNA molecules with oppositely charged lipid membranes. Indeed, on less charged membranes with 3% of DOTAP, we find that the DNA molecules adsorb as coils on membranes but never start entering the grooves, i.e., they never enter the Stage 1 of the dynamics. This is documented in Fig. 6 here. Apparently, between 3 and 5 % of DOTAP, there is an underlying *unbinding transition* of DNA molecules which are here, at low enough DOTAP fractions, unbound from the surfaces grooves while still remaining bound to the membrane surface. We discuss this DNA delocaliza-

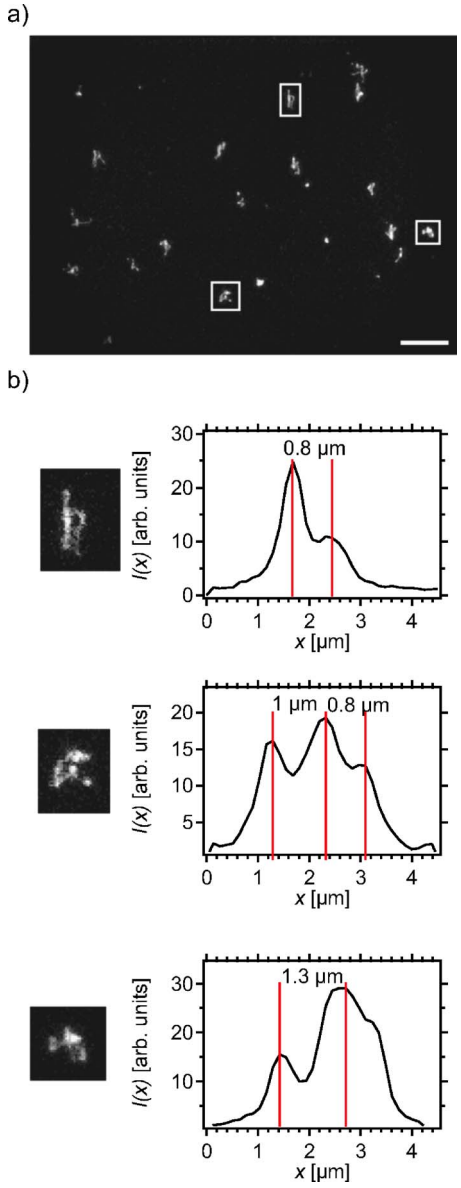

FIG. 6. (Color online) (a) FM images of DNA molecules on periodically structured membrane with 3% of DOTAP (here at $t=180$ min); scale bar=10 μm. Notably, the DNA does not go into the grooves and thus does not stretch. (b) For a few selected molecules, we give the projected intensity profiles $I(x)$.

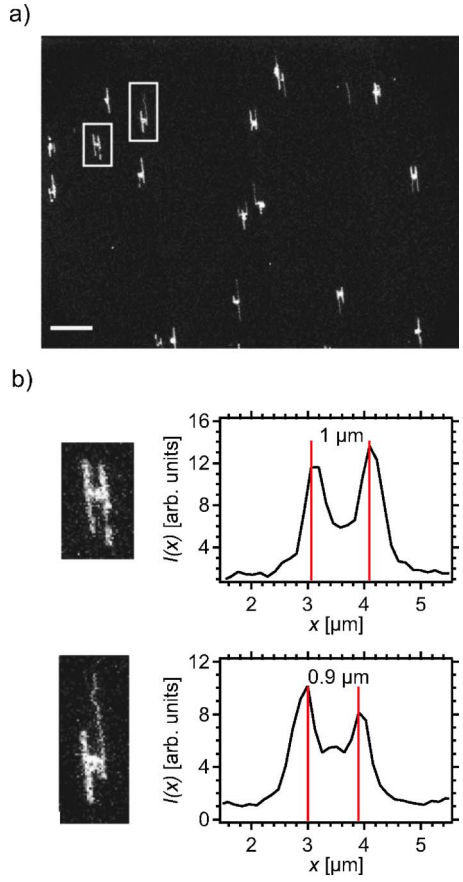

FIG. 7. (Color online) (a) FM images of DNA molecules on periodically structured membrane with 7% of DOTAP (here at $t=185$ min); scale bar=10 μm. (b) For a few selected molecules, we give the projected intensity profiles $I(x)$.

tion phenomenon in the following section. Here, we stress that, to the best of our knowledge, this is the first experimental observation of such semiflexible polymer low-dimensional unbinding phenomena occurring *within a 2D manifold* being the membrane surface in our system.

Interestingly, however, on membranes with 7% of DOTAP, when one would naively expect an even stronger stretching effect than seen at 5%, we find a rather different outcome: Initially, the DNA molecules start vigorously entering the grooves i.e., they enter the Stage 1; see Fig. 7 at 7% of DOTAP. However, this adsorption into grooves eventually halts and, with 7% of DOTAP, at long times the DNA molecules never stretch as much as we see on the membranes with 5% of charged lipid in Fig. 4. There is thus an interesting complexity of these DNA stretching phenomena, marked by an optimum fraction of charged lipids (5% of DOTAP, in the present system at 30 °C) providing the best stretching effect at a given time. We document this feature in Fig. 8 giving the average DNA length projected onto the direction of grooves versus time for various DOTAP fractions.

We use Fig. 8 also to illustrate effects of surface (macroscopic) nonuniformity on the DNA stretching dynamics: On some portions of the surface the observed stretching process was visibly faster whereas on other portions it was slower than average. We attribute these differences to a nonuniformity of the imprinted surface that may have emerged during its fabrication (Sec. II). Indeed, as discussed in the following, the DNA binding effect is quite sensitive to geometrical details of the imprinted surface, such as the curvature of sharp inward curved edges seen in the AFM images in Fig. 2(b). Such fine geometrical details are hard (if not impossible) to keep uniform all over the entire patterned surface, even with a lot of effort done in the fabrication of these surfaces. On the physics side, however, the existence of these surface nonuniformity effects actually serves as indirect yet significant indicator that fine geometrical details *do* play a significant physical role in the here observed DNA stretching process, as discusses in detail in the following.

Another interesting feature seen at 7% of DOTAP (Fig. 7) is the presence of the *H*-shaped DNA configurations [versus

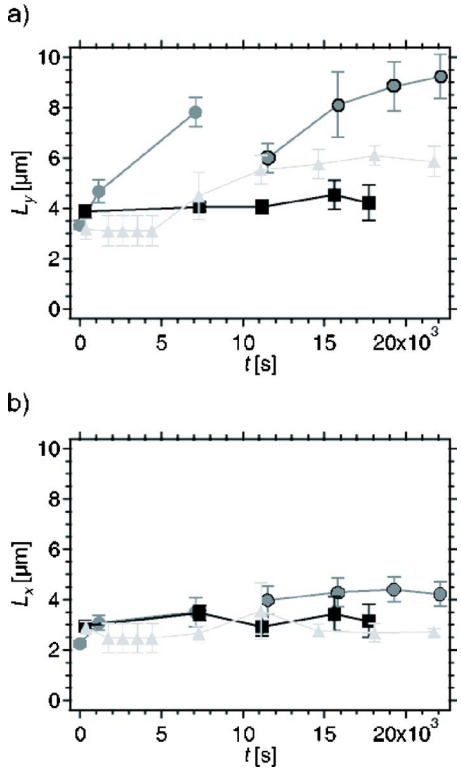

FIG. 8. (Color online) DNA molecules average projection sizes, L_y onto the grooves direction [in (a)], L_x perpendicular to the grooves direction [in (b)] versus time [measured after exchanging the solvent with the salt solution, see Sec. II], as obtained at various DOTAP fractions: 3% (squares), 5% (circles), and 7% (triangles). Note that the DNA stretching effect is at 5% stronger than at *both* 3% and 7% DOTAP. In this figure we illustrate also the effects of macroscopic surface nonuniformity on the DNA stretching dynamics: For the 5% case, the data up to 7000 sec (circles) are obtained at a single surface spot incidentally having somewhat better than average stretching efficiency. On the other side, for $t \geq 11000$ sec, we gave data (enclosed circles) as obtained by averaging over six different surface spots randomly chosen across the entire surface.

the *S*-shaped and *U*-shaped configurations typically seen at 5% of DOTAP in Fig. 4, in addition to the DNA molecules that went into single grooves]. The *H*-shaped configurations seen in Fig. 7 indicate a *double* occupation of some of the grooves therein, with *two* long DNA sections (connected by a small *u* turn) entering the same groove. We elucidate this phenomenon at the end of Sec. IV.

The most important physical question discussed hereafter and in Sec. IV, is on *where* does the DNA molecules actually bind on the surface of the curved membrane? Where are the actual "binding sites" of DNA and what is their physical character? To experimentally address this question, we examine the recorded light intensity distribution coming from the 2D images of DNA molecules in Figs. 3 to 7. This local light intensity $I(x,y)$ is a function of the position (x,y) on the images. A substantial experimental insight into the above posited questions is obtained by using the *projected intensity* $I(x)$ being the sum of $I(x,y)$ over y carried out for a fixed x throughout a domain containing a *single* DNA molecule. Here, as before, the x coordinate is perpendicular to the direction of grooves, so the $I(x)$ is the intensity "projected" along the grooves direction. In Figs. 3 to 7, we include these projected intensities for some of the single molecules in these figures. Interestingly, the most significant information on the DNA binding sites is obtained from the projected intensities $I(x)$ of those single DNA molecules that exhibit two arms sucked into adjacent grooves that are connected by a long DNA crossing section [we recall that such DNA configurations are commonly seen over the Stage 2, see Fig. 4]. Notably from Fig. 4(c), each arm of such a DNA molecule contributes to $I(x)$ a very sharp peak so there are two peaks seen in the projected intensity images of such molecules. The distance between these sharp peaks (along x direction) provides a direct measure between adjacent binding sites of DNA on the microstructure surface. As documented in Figs. 4(c) and 3(b), both obtained at 5% DOTAP, as well as in Fig. 7(b), at 7% DOTAP, we see that the distance between DNA binding sites (measured perpendicular to grooves) is in the range 950–1000 nm. Strikingly, this number coincides with the distance between the inward curved surface edges; see the AFM surface image in Fig. 2(a). Indeed, the separation between the inward curved surface edges [the aforementioned length $L_{long} \approx 950-1000$ nm, see Fig. 2(b)] is the unique prominently visible surface length scale which matches the observed separation between the peaks of the projected light intensity for the molecules in Figs. 3(b), 4(c), and 7(b), and numerous other single DNA molecules with two arms that we have examined in the course of this study. This shows that the actual DNA binding sites are the inward curved edges on the microstructured membrane surface. In this respect, we note that, for example, a putative assumption that DNA binds to outward curved edges in Fig. 2(a) would imply the distance between the projected intensity peaks equal or smaller than 800 nm [see Fig. 2(a)]. However, this is *not* what we see in the $I(x)$ data in Figs. 3(b), 4(c), and 7(b). This rules out the outward curved edges as binding sites of DNA.

Thus, our overall data [AFM surface images and light intensity data] show that DNA binds into the inward curved surface sections, i.e., the inward edges seen in Fig. 2(a). In Sec. IV we discuss the physical origin of this binding potency of the inward curved edges. There, we elucidate also the DNA unbinding (delocalization) transition we saw here to occur between 3 and 5 % of DOTAP. Here, we stress that the projected intensity profiles $I(x)$ obtained at 3% DOTAP in Fig. 6(b) also well evidence that the DNA unbinds form the edges while remaining bound to the membrane. Indeed, the intensity data in Fig. 6(b) are clearly different from those obtained at 5 and 7 % of DOTAP in Figs. 3(b), 4(c), and 7(b) in which the double-peak intensity profiles indicate the presence of well defined binding sites. In contrast to this, the projected DNA light intensity data obtained at 3% DOTAP, Fig. 6(b), are qualitatively similar to those obtained for DNA molecules on *flat* membranes; see Fig. 5(b). This comparison also indicates that the DNA is unbound from the edges on the membranes with 3% of DOTAP, i.e., that DNA molecules undergo an unbinding transition as the DOTAP fraction is decreased from 5 to 3 % DOTAP. We elucidate this phenomenon in the following section.

IV. PHYSICAL ORIGIN OF THE DNA LOCALIZATION AND STRETCHING ON CURVED MEMBRANE SURFACES

Why are the periodically structured charged membranes capable to stretch long DNA molecules? Here, we proceed with physical elucidation of these striking phenomena, and discuss the DNA behavior both at visible long scales and at short scales (<0.4 μm FM resolution). On planar charged membranes, DNA molecules have the shapes of random walks fluctuating in time (see Fig. 5 here, and [9,10]), whereas on the present curved membranes DNA molecules localize and stretch, as in Fig. 4 here. Why? Unlike the planar membranes, the surfaces of curved membranes are (generally) *not* equipotentials. Due to this, a macroion adsorbed on a curved charged surface attains a position dependent free energy, which depends on the *local curvature of the surface*, C. Thus, in particular, a charged rod (DNA) sliding along our one-dimensionally modulated membrane surface, with its axis along the grooves direction, acquires the potential energy of the form

$$U_{ul}(C) = -\Gamma C, \tag{1}$$

per unit length (ul) of DNA. Curvature potential energy in Eq. (1), with $\Gamma > 0$, represents a Mullins-type change of the binding free energy of an adsorbed object due to nonzero C: surface sections with $C > 0$ (curved inward) approach the object more closely and thus bind it *more* strongly than flat surface sections with $C = 0$ [18]; see also Sec. V here. By Eq. (1), Γ has dimension of energy. Γ ranges up to $\approx 5k_BT$ in the present system [19], and, importantly, it can be tuned by changing the fraction of charged lipids. The curvature free energy in Eq. (1) actually represents the difference between the binding free energy (per unit length) of an DNA molecule adsorbed along a charged cylindrical surface *subsection* of a *large* radius $R = 1/C = w/\Theta$ ($\gg$Debye length=1.755 nm here, vs $R \approx 20$ nm for inward curved edges in Fig. 2) and the binding free energy of a DNA molecule adsorbed on a charged plane. Using this, and the Poisson-Boltzmann theory (with mobile surface and spatial charges), we estimate the Γ constant in Eq. (1) to range up to $\sim 5k_BT$ in the present system, depending on charged lipid fraction [19]. In addition to the electrostatic effects, the known packing differences between DOTAP and DOPC head groups are also significant. They tend to enhance positive surface charge (DOTAP) density in the inward curved edges, making Γ in Eq. (1) even more positive [see Sec. V here].

For the present one-dimensionally modulated surface, Eq. (1) yields an interesting potential landscape for DNA, a periodic sequence of potential traps ($C > 0$) and barriers ($C < 0$) as depicted in Fig. 9. Note that there are actually two traps inside of each groove. They occur at highly curved sections of the surface, the *inward curved surface edges* across which the surface slope angle increases quasi-discontinuously by an amount $\Delta\Theta$ over a narrow edge width w, see Figs. 2(b) and 9. From the AFM images in Fig. 2(b), the surface curvature within the edge $C = \Delta\Theta/w \approx 0.035 - 0.045$ nm^{-1}. and $\Delta\Theta \approx 1$ rad, corresponding to the edge width $w \approx 20 - 30$ nm. By Eq. (1), such

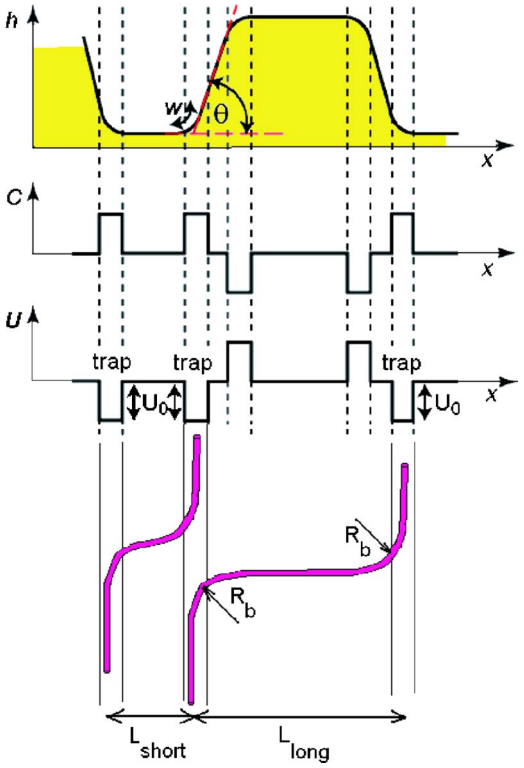

FIG. 9. (Color online) Schematic surface profile $h(x)$, surface curvature $C(x)$, and surface curvature dependent potential energy of DNA, $U(C)$, Eq. (1), along the periodic surface, that forms a sequence of potential traps ($C > 0$) and barriers ($C < 0$). Note that there are actually two traps inside of each groove. They occur at highly curved sections of the surface, the inward curved surface edges at which the surface slope angle quickly increases by the amount $\Delta\Theta$ over the narrow edge width w [see AFM images in Fig. 2(b)]. DNA may form various kinds of crossings between edge traps, such as the long crossings between two traps in neighboring grooves, with the crossing length $L_{long} \approx 970$ nm, and shorter crossings between edge-traps in the same groove, with the crossing length $L_{short} \approx 200$ nm [see also Fig. 2(a)]. On exiting the traps, the DNA makes small nearly circular bends with the radius R_b, see the text.

an inward curved edge yields a *potential trap* (binding well in Fig. 9) with the depth

$$-U_0 = -\Gamma\Delta\Theta/w. \tag{2}$$

This significant finding is in full accord with the experimental data of Sec. III indicating that inward curved edges play role of DNA binding sites. A *single* long edge trap can permanently localize a DNA molecule along it, provided U_0 is big enough to overcome the molecule's positional entropy tending to unbind it from the trap. To elucidate our experimental findings, we consider here the free energy difference between the bound and the unbound semiflexible polymer, of the form,

$$\Delta F_{ul} \approx -U_0 + F_{st}, \tag{3}$$

per unit length. Here, F_{st} is the (steric) free energy of confinement

$$F_{st} = 1.103 \frac{k_B T}{(\xi_{pers}/2)^{1/3} w^{2/3}}, \tag{4}$$

needed to confine a long polymer within a stripe (2D "tube") of the width w [20]; here ξ_{pers} is the polymer persistence length ($\approx$60 nm for our 1:5 labeled DNA, [17]). Thus, by Eq. (3)

$$\Delta F_{ul} \approx -U_0(1-k), \tag{5a}$$

with $k=\frac{F_{st}}{U_0}$ expressed, by Eqs. (2) and (4), as

$$k = 1.103 \frac{k_B T}{\Gamma \Delta\Theta} \left(\frac{w}{\xi_{pers}/2} \right)^{1/3}. \tag{5b}$$

For our experimental values, $\Delta\Theta \approx 1$ rad and $w \approx 20$ nm, Eq. (5b) yields

$$k \approx 0.96 k_B T/\Gamma. \tag{6}$$

For $k<k_c \approx 1$, i.e., $\Delta F_{ul}<0$, the binding energy wins over the entropy ($U_0>F_{st}$), and the polymer remains localized inside the edge. Conversely, for $k>k_c \approx 1$, i.e., $\Delta F_{ul}>0$, the entropy wins over binding energy ($F_{st}>U_0$), and the polymer unbinds from the edge (while *still* bound to the membrane) to eventually assume the shape of a 2D self-avoiding random walk. In the present system, $k \approx k_B T/\Gamma \approx 0.2$ at high surface charge densities, and it increases with decreasing amount of charged lipids [19], allowing to cross the DNA unbinding transition at $k_c \approx 1$. Indeed, our experiments show that on 5% DOTAP membranes the DNA still binds to the edges [Fig. 4], while on 3% DOTAP membranes we find that the deposited DNA does not enter the edges [see Fig. 6]. Our experimental results thus provide, to our knowledge, the very first observation of a single semiflexible polymer unbinding transition on a 2D manifold, in which DNA molecules unbind from one-dimensional attractive manifolds (edges) while remaining bound to two-dimensional manifolds (membranes).

We note that semiflexible polymers confined to a plane and attracted by a *single* potential well (e.g., a columnar defect) exhibit a true second order unbinding transition [21]. For rectangular wells (as in Fig. 9), recent Monte Carlo (MC) simulations of Gao and one of us [22], show that the critical value of k is $\cong$1.5. In the present interesting bound phase (in which the DNA localizes and thus stretches) the simple statmech picture employed here via Eq. (3) is (asymptotically) exact for $k<1$ [22].

Above, we focused on the effects of a single edge potential trap whereas on our surfaces we have a periodic sequence of such edge-traps seen in Fig. 9. These traps are competing with each other to capture DNA. Due to this, a very long polymer may still maintain an *anisotropic* random walk shape even for $k<k_c$ by developing *crossings* between different attractive edges (see Fig. 9). In our experiments we indeed observe that such crossings form *initially* but then tend to disappear at long times, so that DNA eventually stretches in equilibrium. See the images in Fig. 4, taken within Stage 2 of the DNA evolution, in which we can still see the long DNA crossings between the grooves, with the length $L_{cross}=L_{long} \approx 1$ μm (the distance between inward curved edges in different grooves; see Fig. 2 and discussions in Sec. III). What ensures the experimentally observed extinction of these long crossings and the resulting DNA stretching? To elucidate this effect, we note that the presence of such a crossing along the polymer introduces an extra free energy cost (relative to the polymer configuration completely bound to a single edge) of the form $\Delta F_{cross}=\sigma L_{cross}$. Here, the *line extraction tension* $\sigma=-\Delta F_{ul}$ is the free energy cost to unbind unit length of the polymer from the edge trap. It is positive in the bound polymer state ($k<k_c$). In thermal equilibrium, the crossings between traps *must* form along a *long enough* polymer: By analogy to thermally activated domain walls in 1D systems [23], the equilibrium separation between the crossings along the polymer contour behaves as

$$\xi_{cross} \sim \exp(\Delta F_{cross}/k_B T) = \exp(L_{cross}/l_\sigma). \tag{7}$$

Here, l_σ is a capillary length given by $l_\sigma=k_B T/\sigma \approx w(k_B T/\Gamma\Delta\Theta)/(1-k)$ [for $\sigma=-\Delta F_{ul}$ as in Eq. (5a)]. Unless very close to the DNA unbinding transition at $k=k_c \approx 1$, the capillary length $l_\sigma<w \approx 20-30$ nm, so l_σ is 50–30 times smaller than the length L_{cross} of the $L_{long} \approx 1000$ nm long DNA crossings between the grooves. Thanks to this large separation between the length scales L_{cross} and $l_\sigma \sim w$=edge width, the average *equilibrium* distance between such crossings, $\xi_{cross} \sim \exp(L_{cross}/l_\sigma)$ is very large for the long DNA crossings. For a realistic finite size polymer, this means there will be no such crossings between grooves once the thermal equilibrium is reached. Due to this, the 1 μm long crossings in Fig. 4 irreversibly disappear at long times, during the Stage 2 over which DNAs move into single grooves and thus stretch, as best seen at 5% DOTAP fraction. Note that on our surface, DNAs can also make short crossings between the two edge-traps in the *same* groove (see Figs. 2 and 9), with $L_{cross}=L_{short} \approx 200$ nm, about five times shorter than the length of the long DNA crossings between *different* grooves, with $L_{cross}=L_{long} \approx 1000$ nm. Therefore, in principle, nonequilibrium and equilibrium densities of the short crossings might be significant and responsible for the fact that the DNA projected length (along the grooves direction) is smaller than the total DNA contour length of 22 μm, even for the DNAs completely adsorbed into single grooves which have projected lengths $\approx 13-14$ μm [for 5% DOTAP, see Fig. 4]. However, by simple geometry, it can be seen from Fig. 2(a) that, for the DNA molecules with two arms, a significant density of the short crossings would yield bimodal projected light intensity profiles $I(x)$ with interpeak separation=1170 nm=surface period, versus the actually observed peak separation $\approx 950-1000$ nm [see Sec. III, and Fig. 4(c)]. This experimental fact rules out a substantial density of short crossings on the DNA molecules in our 5% DOTAP experiments. The observed projected DNA projected lengths are thus governed by the transverse fluctuations of DNA molecules around *single* traps. Indeed, at 5% DOTAP, the presence of substantial transverse polymer fluctuations is to be expected, having in mind the proximity of the DNA unbinding transition that occurs between 3 and 5% of DOTAP [see Sec. III].

It is significant to compare the long DNA crossings seen in our experiments [Figs. 3 and 4] to the hairpin turns formed

along a semiflexible polymer that is *orientationally* coupled to a nematic solvent, [24]. In contrast to this model system, the major role in our experimental system is played by the *positional* coupling of the polymer to the periodic sequence of edge traps. Moreover, in contrast to the hairpin turns of Ref. [24], the polymer bending elastic energy plays a minor role in the physics of our long DNA crossings. It gives only a subdominant contribution to the free energy cost of a long DNA crossing, which turns out to be dominated by the line extraction tension σ. To see this, note that, on exiting the traps, the DNA should make small nearly circular sections (bends) where the bending elastic energy is mostly concentrated [see Fig. 9]. There are two nearly circular bends per each DNA crossing, and estimates for the bends radius R_b and their contribution to the net crossing energy are easily obtained by minimizing the *net* crossing free energy =extraction tension free energy of the whole crossing length+bending elastic energy of the *two* bends. By simple geometry, the presence of a crossing extracts the DNA length$=L_{cross}-2R_b+\pi R_b$ [see Fig. 9]. Thus, the net crossing energy has the form

$$\Delta F_{cross} = \sigma(L_{cross} - 2R_b + \pi R_b) + \pi R_b \frac{\pi\kappa}{2R_b^2}, \tag{8}$$

with $\kappa=k_BT\xi_{pers}/2$, the DNA bending constant contributing the second, bending elasticity term to Eq. (8). Minimizing the free energy (4) over R_b yields $R_b=[\pi/4(\pi-2)]^{1/2}(l_\sigma\xi_{pers})^{1/2}\sim 30$ nm (as $l_\sigma\sim w\sim 20$ nm), and the net crossing energy in the form $\Delta F_{cross}=\Delta F^{(\sigma)}_{cross}+\Delta F^{(\kappa)}_{cross}$. Here, the first contribution is, as before, $\Delta F^{(\sigma)}_{cross}=\sigma L_{cross}=k_BT(L_{cross}/l_\sigma)$, the extraction tension contribution to the crossing energy, which is $\sim 50k_BT$ for the long crossings between grooves, with $L_{cross}\approx 1$ μm. The second contribution to ΔF_{cross} is due to the bending elasticity and has the form $\Delta F^{(\kappa)}=k_BT[\pi(\pi-2)]^{1/2}(\xi_{pers}/l_\sigma)^{1/2}\sim 3.5k_BT$. Thus, $\Delta F_{cross}\approx\Delta F^{(\sigma)}_{cross}\gg\Delta F^{(\kappa)}_{cross}$, showing that for our long DNA crossings bending elasticity plays only a minor role relative to that of the extraction tension.

At this point, it is illuminating to note that, *if* overhangs would be artificially forbidden along the polymer contour length, the present statistical mechanics problem, with a periodic sequence of traps and polymer crossings going between the traps, would become closely related to the statistical mechanics of the well known 1D interface roughening the solid-on-solid (SOS) model [25]. This interface model is equivalent to the familiar directed polymer model in 1+1 dimensions [25], which transverse wandering would be governed here by a tension proportional to our line extraction tension σ. It is because the semiflexible polymer acquires here the (extraction) tension energy along the DNA crossing sections that are outside the traps. Moreover, as for directed polymers, the polymer bending elasticity plays a secondary role here, as we discussed above. Directed polymers as well as the 1D interface roughening model without overhangs are both known to be in the rough (wandering) phase at any temperature. By this analogy, no true polymer localization to a single trap is expected in our system, i.e., a long enough polymer remains in the delocalized phase by making crossings between the multitude of attractive wells competing to capture the polymer. On the other side, going beyond the directed (SOS) polymer models, overhangs are actually *not* forbidden in our system (see, e.g., DNA "*U* turns" in Fig. 4). This feature increases positional *and* orientational disorder of the polymers here, making the true localization even more suppressed in the thermodynamic limit of *very long* polymers. Due to the overhangs, long enough polymers will exhibit an *anisotropic* random walk behavior in thermal equilibrium, with two kinds of segments: the crossings between traps [of the length L_{cross}], and much longer segments along the traps [with the average length $\xi_{cross}\sim\exp(L_{cross}/l_\sigma)$], as discussed before. Nonetheless, in spite the absence of true polymer localization for long polymers, a *finite size* polymer shorter than our length scale ξ_{cross}, will be localized around single potential trap (and thus "stretched") in thermodynamic equilibrium (much like, e.g., a finite size 1D Ising model has, effectively, a quasilong-range order, ferromagnetic phase such as behavior at low T, if its size is smaller than the correlation length). This fact plays the paramount role in the physics of the here explored phenomena.

In practical terms, the revealed DNA stretching effect relies also on the kinetic ability of DNA to reach its thermal equilibrium shape within experimentally accessible time scales. Interestingly, as found in the experiments of Sec. IV, increasing the charged lipid fraction above 5% *increases* the stretching time scale, and may even prevent the DNA to ever enter the stretching Stage 2. Indeed, on 7% DOTAP membranes, we find that the Stage 2 is pre-empted by a halt of the Stage 1 process [see Fig. 7]: the initially formed small DNA globules release arms growing into grooves, but then the arms growth is halted. This halt appears to be caused by energy barriers clogging the edges for the DNA advance. The barriers can be produced by the surface curvature *along* the direction of edge traps, i.e., longitudinal imperfections of (otherwise straight) grooves, see Fig. 1(b). Like to the curvature potential of the (more curved) edge traps, a weaker curvature potential contributed by the (less curved) longitudinal imperfections also increases with increasing DOTAP %, which eventually closes the edges for the DNA passage. Due to this, by increasing the DOTAP % above the critical value for the DNA unbinding-from-edges transition (at $\approx$3% of DOTAP), the stretching effect enhances only initially, up to 5% of DOTAP (at 30 °C), which turns out to be the *optimum* charged lipid fraction, providing the minimum DNA stretching time [see Fig. 8]. Further increase of DOTAP % only slows down (and eventually halts) the DNA stretching.

Another interesting feature of the DNA localization, revealed at higher DOTAP fractions, is the *multiple occupation* of DNA molecules inside the potential traps. We recall Fig. 7, obtained at 7% of DOTAP, in which *H*-shaped DNA molecules are seen. Such configurations can be realized only if some of the traps are double occupied by two long DNA sections both localized inside the *same* trap. The phenomenon of multiple occupation of the traps is of a fundamental interest here. It is a demonstration of the strong dependence of the adsorption efficiency of the edge traps on the DOTAP fraction, i.e., on the strength of electrostatic interactions encoded in our curvature potential, Eq. (1) that regulates the depth of traps, Eq. (2). Indeed, at 5% of DOTAP, the data in

Fig. 4 show that all the traps are single occupied (occupation number $N=1$), whereas at the higher 7% DOTAP fraction we observe the double occupation ($N=2$) of the traps as seen on *all* the molecules in Fig. 7 (which are all H-shaped). Finally, at low DOTAP fractions, such as 3% in Fig. 6, there are no long DNA sections inside the traps, corresponding to the occupation number $N=0$. Our data thus indicate that with increasing DOTAP fraction one has a sequence of phase transitions between thermodynamic states characterized with different occupation numbers $N=0,1,2,\ldots$, of the long DNA sections that can be *stacked in parallel* in the same edge trap. To elucidate these practically important and theoretically interesting phase transition phenomena, let us consider a smectic stack of N repelling semiflexible polymers (N smectic layers) confined in the same trap of the width w [26]. It is straightforward to generalize the free energy (per unit length) stated in Eq. (3) for $N=1$ to any N

$$\Delta F_{ul}(N) \approx -NU_0 + NF_{st}^{(1)}(w^{(1)}), \tag{9}$$

with U_0 as in Eq. (2), whereas the steric free energy $F_{st}^{(1)}$ has the form as in Eq. (3), however with the trap width w replaced by $w^{(1)}$, representing the effective width of the tube available for the single layer transverse fluctuations

$$w^{(1)} = \frac{w}{N} - D_{eff}, \tag{10}$$

i.e.

$$F_{st}^{(1)}(w^{(1)}) = 1.103\frac{k_BT}{(\xi_{pers}/2)^{1/3}\left(\frac{w}{N} - D_{eff}\right)^{2/3}}. \tag{11}$$

D_{eff} in Eqs. (10) and (11) is an effective DNA diameter [26]. With purely steric interactions, D_{eff} would coincide with the molecule's steric diameter=2 nm for DNA. In the case of strongly charged molecules such as DNA, the effective diameter is bigger than the steric diameter by an amount comparable to the Debye screening length=1.755 nm in the present experimental system. Thus, $D_{eff}\approx 4$ nm is a reasonable estimate. Note also that, for our traps with $w\approx 20$ nm (or bigger), the effect of such an D_{eff} in Eq. (11) is weak for small N values ($N=1$ or 2). Yet, by Eq. (11) it is clear that a nonzero D_{eff} imposes an upper limit on the number of smectic layers that can be (in principle) stored in a single trap

$$N_{\max} = w/D_{eff}. \tag{12}$$

Thus, for our traps, with $w\approx 20-25$ nm and $D_{eff}\approx 4$ nm, this maximum number of layers is $N_{\max}\approx 6$. By Eqs. (9)–(12), the stack free energy assumes the form

$$\Delta F_{ul}(N) \approx U_0\left(-N + k\frac{N^{5/3}}{(1-N/N_{\max})^{2/3}}\right), \tag{13}$$

with the parameter k introduced before in Eq. (5b). We recall that for our experimental system $k\approx k_BT/\Gamma$; see Eq. (6). By Eq. (13), the N layers stack free energy becomes negative for

$$k < k_{bound}(N) = \frac{(1-N/N_{\max})^{2/3}}{N^{2/3}}, \tag{14}$$

indicating that the whole stack is then bound to the trap. The bound states with different numbers of layers $N=0,1,2,3,\ldots,N_{\max}$ compete with each other, and, for a given value of the parameter k, the integer N minimizing the free energy (13) will win. By this fact, using Eq. (13), we find the sequence of phase transitions $N=0\rightarrow N=1\rightarrow N=2\rightarrow N=3\rightarrow\cdots$ occurring with decreasing k, i.e., increasing Γ. The transition $N\rightarrow N+1$ occurs when $\Delta F_{ul}(N)=\Delta F_{ul}(N+1)$ yielding, by Eq. (13), the critical value for k at this transition, in the form

$$k_c(N\rightarrow N+1) = \left[\frac{(N+1)^{5/3}}{[1-(N+1)/N_{\max}]^{2/3}} - \frac{N^{5/3}}{[1-N/N_{\max}]^{2/2}}\right]^{-1}. \tag{15}$$

To relate this result to our experiments, we note that Eq. (15), with $N_{\max}=6$, yields the sequence of transitions at

$$k_c(0\rightarrow 1)=0.855, k_c(1\rightarrow 2)=0.331, k_c(2\rightarrow 3)=0.174, \ldots .$$

Note that the $N=2\rightarrow N=3$ transition, as well as all subsequent transitions, occur at the values of $k\approx k_BT/\Gamma$ that are smaller than the minimum value k that occurs in our electrostatic system ($k_{\min}\approx 0.2$ for $\Gamma_{\max}\approx 5k_BT$ [19]). Thus, within the $w\approx 20$ nm wide traps, one can confine a small stack with up to $N=2$ layers. The states with $N=1$ layer, realized with 5% of DOTAP (Fig. 4) occur for the parameter k in the range $k_c(0\rightarrow 1)=0.855>k>k_c(1\rightarrow 2)=0.331$, corresponding to the parameter Γ in the range to $\Gamma_c(0\rightarrow 1)\approx k_BT<\Gamma<\Gamma_c(1\rightarrow 2)\approx 3k_BT$. The double occupied states with $N=2$ smectic layers occur for k in the range $k_c(1\rightarrow 2)=0.331>k>k_c(2\rightarrow 3)=0.174$, corresponding to Γ in the range $\Gamma_c(0\rightarrow 1)\approx 3k_BT<\Gamma<\Gamma_c(1\rightarrow 2)\approx 6k_BT$. This range is captured (on the lower side) in our experiments at 7% of DOTAP (Fig. 7) as evidenced by the presence of the H-shaped DNA molecules indicating the double occupation of the traps. Our simple theory, based on the physics of sterically stabilized smectic stacks [26], thus provides a sound explanation for the multiple DNA occupation of the traps seen in the experiments.

We stress that the above discussions assume long polymer sections, i.e., the thermodynamic limit of long "smectic layers" in which case one can ignore the finite size effects of the lateral boundaries of the stack. For example, if the smectic stack is formed out of N sections of a single DNA molecule that has folded $N-1$ times while being adsorbed into a single trap (with each fold producing a smectic layer), then, for long enough layers, one can ignore the energy contribution coming from the short u-turns connecting neighboring smectic layers at their lateral boundaries. Adding u-turns bending energies to the system free energy Eq. (9) would not affect the above conclusions if the smectic layers are long [see, e.g., our discussions of Eq. (8)]. It should be stressed that the previous discussions assume that the smectic layer length

(size of the smectic stack base) is constrained to have a fixed value. However, obviously, this length is allowed to change due to the unfolding of the polymer *inside* the trap. By assuming purely repulsive polymer self-interaction, the folded polymer (with free ends) will unfold to eventually assume the configuration of a single smectic layer $N=1$. Thus, the bound smectic like states with $N>1$ are, in principle, unstable. These states are however long lived if the polymer unfolding dynamics is slow. Indeed, within the narrow edge traps, the DNA unfolding can be kinetically prohibited by the energy barriers hindering the motion of the small DNA u-turns which connect neighboring smectic layers at their boundaries. The *u*-turns motion (DNA unfolding) can be halted by energy barriers clogging the edge traps. As noted earlier in this section, such barriers emerge due to the surface curvature along the direction of edge traps, and the barriers heights increase with increasing DOTAP fraction (as evidenced by our experiments with 7% of DOTAP in Fig. 7). Due to the barriers, the multiple folded (smecticlike) DNA states ($N>1$) may become effectively stable on the experimental time scales. At same time, with increasing DOTAP %, these smecticlike DNA conformations become energetically favored, as discussed above. In effect, a single DNA molecule may easily fold over itself while being adsorbed into an edge trap. The base size (along the edge trap) of such a smectic stack is the same as the separation between the barriers which are high enough to kinetically prohibit the DNA unfolding inside the edge trap. It is significant to stress that this barrier separation (and thus the stack base size) decreases with increasing DOTAP fraction which regulates the height of the energy barriers. Thus, in our experiments at 5% of DOTAP, the barrier separation is large enough to allow the whole DNA molecules to enter traps without folding (i.e., an $N=1$ stack forms inside the traps). On the other hand, at 7% of DOTAP, the barrier separation was sufficiently small to cause the observed DNA folding (i.e., the existence of the $N=2$ stacks bound to traps in Fig 7).

For the future experiments, it is illuminating to note that (with an appropriate master geometry) one can easily create arrays of traps which are *shorter* than the DNA molecules length, e.g., a few microns long traps. Such a trap would act as a *tag* by adsorbing only a portion of the DNA contour length whereas the rest of it would remain as a free tail outside the trap. Interestingly, the adsorbed DNA portion can be made longer than the trap length. Indeed, the adsorbed DNA section can fold inside the trap and thus form a smectic stack with the base size equal to the trap length. Moreover, by our discussions here [see Eq. (15)], the adsorbed DNA section length (determined by the number of the adsorbed smectic layers) and thus also the free tail length can controlled by the DOTAP fraction. This would provide a way to engineer a novel type of molecular tags that would allow for *controllable* sizes of the free molecular tails.

V. SUMMARY AND DISCUSSIONS

In summary, the statistical physics of semiflexible polymers adsorbed on periodic membranes encompasses the conceptually and practically interesting phenomena of polymer localization and coil stretching revealed in our experiments with DNA. On the practical side, in contrast to presently employed micro-fluidic methods [12], our new approach to stretch DNA coils avoids any use of fluid flows and the throughput limitations due to the difficulties in entering DNA into microfluidic channels. Indeed, the DNA can be easily brought in large amounts onto our periodic membranes. Additionally, the stretched DNA molecules are freely exposed to a larger surrounding water medium and all the molecules dissolved in it. Due to this feature, our new way to stretch polyelectrolytes may facilitate more direct, high throughput protocols and experimental studies of fundamental biological interactions between DNA and other biomolecules.

Our study has highlighted the previously un-anticipated significant role of surface curvature potentials in governing conformations of biomacromolecules. These effects are prone to play an important role in future biophysical and biotechnological studies. We comment here more on the physical nature of these effects capable of binding adsorbed charged molecules into inward curved surface sections. This effect, encoded in our Eq. (1) with a *positive* Γ, is of the same nature as the Mullins type attraction of ad-atoms to positively (inward) curved sections on the surfaces of solids [18]. In the present context, with screened electrostatic interactions, the inward curved sections ($C>0$) on the positively charged membrane produce a focusing of electric field lines above the membrane. This curvature effect yields an enhancement of the local electrostatic potential above positively curved inward edges, i.e., a *positive* curvature potential [19]. Such a positive curvature potential attracts *negatively* charged adsorbed ions (or macroions such as DNA) into the inward curved surface sections. At the same time however, the curvature potential will naturally cause a certain depletion of mobile *positively* charged lipids (DOTAP) in these inward curved edges. Likewise, a negative curvature potential that occurs above the outward curved edges tends to repel negative ad-ions, and, as well, to cause an enhancement of positively charged lipids in the outward curved edges. One may thus naively suspect that such a redistribution of positively charged lipids may be strong enough to attract the negatively charged ad-ions (such as DNA) to go into outward curved edges. Such a guess however turns out to be wrong. The charge redistribution of positively charged lipids is *not* capable to reverse the *sign* of the curvature potential (at the mean-field level, at least). This can be easily seen by recalling that the positive lipid charge distribution is itself governed by the usual mean-field Boltzmann formula (with the curvature potential as its entry!). Indeed, if the charge redistribution ("demixing") would somehow change the sign of curvature potential, then (by the Boltzmann formula), such a demixing would suppress (kill) itself. This argument shows that the most what can be caused by lipid charge redistribution is a certain softening of curvature potentials (relative to the model with immobile surface charges of fixed density). As a quantitative example for this, from the Poisson-Boltzmann calculations [19] (that can be done both with immobile and mobile charges), at 5% DOTAP, at 30 mM salt (Debye length=1.755 nm), these mobile surface charge redistribution effects soften the curvature

potential at the height=1 nm above the membrane by the factor 0.7, relative to the model with immobile charges. Overall, such a curvature induced surface charge redistribution plays only a quantitative role, and, as a matter of principle, it is *not* itself capable to produce sign reversal of the curvature potential.

In fact, a much more significant charge demixing effect in the present cationic membrane system is the well-known demixing of positive lipids induced by presence of highly negatively charged ad-ions such as DNA here. It is experimentally well known that DNA adsorbed on cationic membranes is capable to significantly increase the amount of positively charged mobile lipids in its vicinity; see Ref. [10]. This charge demixing effect strongly amplifies the overall attraction of the DNA to the surface and thus enhances also the attraction of DNA to the inward curved sections, simply because these sections approach the DNA more closely and thus bind it more strongly than flat surface sections or outward curved surface sections, as encoded in our Eq. (1) with a positive Γ.

Next, let us comment on demixing (charge redistribution) effects due to *lipid contrast* (steric and residual electrostatic differences) between DOTAP and DOPC molecules. In our considerations of the choice of lipids, we have taken into account the known segregation trends due to the contrast between charged (DOTAP) and polar lipid (DOPC). In the present system, both lipids are DO (Dioleoyl) lipids, meaning they have identical carbon tails and glycerol group, so the lipid contrast is dominated by the differences between their head groups: small charged TAP head (monopole) with a short backbone (2–3 Å), versus bigger polar PC heads (dipole) having a much longer backbone (10 Å) ending with a large nitride group. Due to having such a large and strongly fluctuating head, the *neutral* lipid DOPC prefers migrating into outward curved surface sections and, likewise, it does not like migrating into inward curved sections. On the other side, the head of the *charged* lipid DOTAP is small and has no such curvature preferences. In fact, these differences are already recognized in literature, frequently describing charged DOTAP as nearly "cylindrically" shaped molecule (nearly no preferred curvature), whereas neutral DOPC molecule is described as *inverted truncated cone* (with upper base, on water side, wider than the lower base) so it prefers going to outward curved membrane sections and it does not like going into inward curved sections. In view of these facts, it is clear what happens on the significant outer leaf of our DOTAP-DOPC membranes (with small DOTAP fraction, as actually used in our study): On the outward curved section, it is energetically favorable to *substitute* DOTAP molecule by a DOPC molecule. Hence, the DOTAP density tends to be depleted on the outward curved sections. Likewise, due to the same reasons, DOTAP density tends to be enhanced on the inward curved edges. Thus, the lipid contrast (between DOTAP and DOPC) itself enhances the positive surface charge density on the inward curved membrane surface sections, and this actually favours the binding of negatively charged ad-ions such as DNA into inward curved sections of DOTAP-DOPC bilayers.

ACKNOWLEDGMENTS

We thank H. Lorenz, C. Meyer (CeNS), and V. Kahl, U. Rädler (ibidi GmbH) for help at various stages of this project. M.B.H., J.A.L., and J.O.R. acknowledge the support through SFB 563. L.G. thanks the DAAD for the Grant No. A/02/15054 sec.315.

[1] P. L. Felgner *et al.*, Proc. Natl. Acad. Sci. U.S.A. **84**, 7413 (1987).
[2] J. O. Rädler, I. Koltover, T. Salditt, and C. R. Safinya, Science **275**, 810 (1997).
[3] T. Salditt, I. Koltover, J. O. Rädler, and C. R. Safinya, Phys. Rev. Lett. **79**, 2582 (1997); Phys. Rev. E **58**, 889 (1998).
[4] L. Golubović and M. Golubović, Phys. Rev. Lett. **80**, 4341 (1998).
[5] C. S. O'Hern and T. C. Lubensky, Phys. Rev. Lett. **80**, 4345 (1998).
[6] F. Artzner, R. Zantl, G. Rapp, and J. Rädler, Phys. Rev. Lett. **81**, 5015 (1998).
[7] L. Golubović, T. C. Lubensky, and C. S. O'Hern, Phys. Rev. E **62**, 1069 (2000).
[8] E. Sackmann, Science **271**, 43 (1996).
[9] B. Maier and J. O. Rädler, Phys. Rev. Lett. **82**, 1911 (1999).
[10] B. Maier and J. O. Rädler, Macromolecules **33**, 7185 (2000).
[11] M. B. Hochrein, J. A. Leierseder, L. Golubović, and J. O. Rädler, Phys. Rev. Lett. **96**, 038103 (2006).
[12] See R. H. Austin *et al.*, Phys. Today **50**, 32 (1997); J. O. Tegenfeldt *et al.*, Proc. Natl. Acad. Sci. U.S.A. **101**, 10979 (2004); W. Reisner, K. J. Morton, R. Riehn, Y. M. Wang, Z. Yu, M. Rosen, J. C. Sturm, S. Y. Chou, E. Frey, and R. H. Austin, Phys. Rev. Lett. **94**, 196101 (2005).
[13] T. Nielsen *et al.*, J. Vac. Sci. Technol. B **22**, 1770 (2004).
[14] T. Pompe *et al.*, Langmuir **15**, 2398 (1999).
[15] C. Miller, P. Cuendet, and M. Grätzel, J. Electroanal. Chem. Interfacial Electrochem. **278**, 175 (1990).
[16] M. B. Hochrein, C. Reich, B. Krause, J. O. Rädler, and B. Nickeł, Langmuir **22**, 538 (2006).
[17] T. T. Perkins, D. E. Smith, R. G. Larson, and S. Chu, Science **268**, 83 (1995).
[18] See W. W. Mullins, J. Appl. Phys. **28**, 333 (1957); in *Metal Surfaces: Structure, Energetics and Kinetics* (American Society for Metals, Metals Park, OH, 1963), p. 17.
[19] L. Golubovic (unpublished).
[20] T. W. Burkhardt, J. Phys. A **30**, L 167 (1997).
[21] R. Bundschuh and M. Lässig, Phys. Rev. E **65**, 061502 (2002); R. Bundschuh, M. Lässig, and R. Lipowsky, Eur. Phys. J. E **3**, 295 (2000).
[22] L. Gao and L. Golubovic (unpublished).
[23] See, L. D. Landau and E. M. Lifshits, *Statistical Physics* (Pergamon, Oxford, 1969).
[24] D. R. Nelson, *Defects and Geometry in Condensed Matter Physics* (Cambridge University Press, 2002). See Ch. 9 and references therein.

[25] For review, see *Statistical Mechanics of Membranes and Surfaces*, edited by D. R. Nelson, T. Piran, and S. Weinberg (World Scientific, 1989). See also Ref. [24], Chapters 7, 8, and 9.

[26] For related discussions, see L. Gao and L. Golubovic, Phys. Rev. E **66**, 051918 (2002); **67**, 021708 (2003); **68**, 041907 (2003). The numerical prefactor in Eq. (11) generally depends on the number of polymers in the stack of N semiflexible polymers confined (in a plane) between hard walls at the distance w. This prefactor is 1.103 for $N=1$ (as found by Burkhardt in Ref. [20]), whereas it is 0.648 for extensive smectic phase stacks with infinite N [as found in L. Gao and L. Golubovic, Phys. Rev. E **66**, 051918 (2002); see the Eq. 4.1 therein]. For other values of N, the value of the prefactor has not been calculated thus far. However, in the present system with relatively narrow traps (and thus with only a small number of polymers that can be stored in such traps) employing the prefactor's value as for $N=1$, as done on Eq. (11), is reasonable.